Acta Crystallographica Section B
Structural Science
ISSN 0108-7681

Reversible dimerization of C_{60} molecules in the crystal structure of the bis(arene)chromium fulleride $[Cr(C_7H_8)]_2C_{60}$

Andreas Hönnerscheid, Robert Dinnebier and Martin Jansen*

Max-Planck-Institut für Festkörperforschung, Heisenbergstrasse 1, 70569 Stuttgart, Germany

Correspondence e-mail: m.jansen@fkf.mpg.de

Received 25 January 2002
Accepted 30 January 2002

Bis(toluene)chromium fulleride, $[Cr(C_7H_8)_2]C_{60}$, has been synthesized as a black microcrystalline powder from C_{60} and $[Cr(C_7H_8)_2]$ in toluene. $[Cr(C_7H_8)_2]C_{60}$ is an ionic compound in which the fullerene is negatively charged and the bis(toluene)chromium molecule positively charged. At T = 250 K a reversible first-order phase transition from a primitive cubic high-temperature phase to a triclinic low-temperature phase occurs. The high-temperature phase [$Pm\bar{3}m$, a = 9.9840 (1) Å, T = 295 K] is composed of dynamically disordered fulleride anions and bis(toluene)chromium(I) cations in a CsCl-type arrangement. The triclinic low-temperature modification [$P\bar{1}$, a = 13.6414 (8), b = 13.8338 (7), c = 13.8548 (7) Å, α = 91.830 (3), β = 116.776 (2), γ = 119.333 (2)°, T = 235 K] consists of ordered C_{60} dimers and two crystallographically distinct bis(toluene)-chromium entities.

1. Introduction

One outstanding feature (among others) of C_{60} is its ability to aggregate *via* covalent bonds in different oxidation states (Iwasa *et al.*, 1994; Stephens *et al.*, 1994). During photochemical or high-pressure reactions of neutral C_{60}, polymers form by [2 + 2] cycloaddition (Rao *et al.*, 1993; Oszlányi & Forró, 1995). The monoanionic alkali metal fullerides AC_{60} (A = K, Rb, Cs) display monomers, dimers or polymers, respectively, depending on the thermal history of a given sample (Chauvet *et al.*, 1994; Stephens *et al.*, 1994; Núñez-Regueiro *et al.*, 1995; Fox *et al.*, 1996; Oszlányi *et al.*, 1996). At elevated temperatures (>500 K) a rocksalt-type face-centered cubic (f.c.c.) structure with rotationally disordered C_{60} anions exists. On slow cooling below 380 K polymerization occurs *via* [2 + 2] cycloaddition, whereas $(C_{60})_2^{2-}$ dimers form on quenching of the f.c.c. phase. More recently, Prassides and coworkers attributed the loss of cubic symmetry in mixed A_3C_{60} fullerides to a linking of the C_{60} anions (Prassides *et al.*, 1997). The first example of a two-dimensional fulleride polymer has been observed in Na_4C_{60}, where each C_{60} is connected to its four in-plane neighbors by four single bonds (Oszlányi *et al.*, 1997). It is important to note that the crystal structures of most fullerides under investigation so far are based on a f.c.c. packing of the C_{60} molecules.

Here we present results on the monoanionic fulleride $[Cr(C_7H_8)_2C_{60}]$. In this compound the transition metal chromium is incorporated as a low-valent bis(toluene) complex. On unifying the closed-shell species C_{60} and bis(toluene)-chromium, both dissolved in toluene, a solid containing the

reactants in an equimolar ratio precipitates. Unexpectedly, the product is not a co-crystallisate; instead a single electron transfer from bis(toluene)chromium to C_{60} occurs, resulting in the ionic compound $[Cr(C_7H_8)_2]^+C_{60}^-$.

$[Cr(C_7H_8)_2]C_{60}$ has been investigated by several spectroscopic methods including NMR and ESR spectroscopy, as well as static magnetic measurements (SQUID), see Hönnerscheid *et al.* (2001). All these methods provide clear evidence for a dimerization of the C_{60}^- anions during a reversible first-order phase transition, occurring at $T \simeq 250$ K. However, the definite proof of the dimerization of the C_{60} molecules by crystal structure determination is still lacking. All attempts to grow single crystals of sufficient quality for X-ray single-crystal investigations failed so far. Therefore, we decided to determine the crystal structure from high-resolution X-ray powder diffraction data.

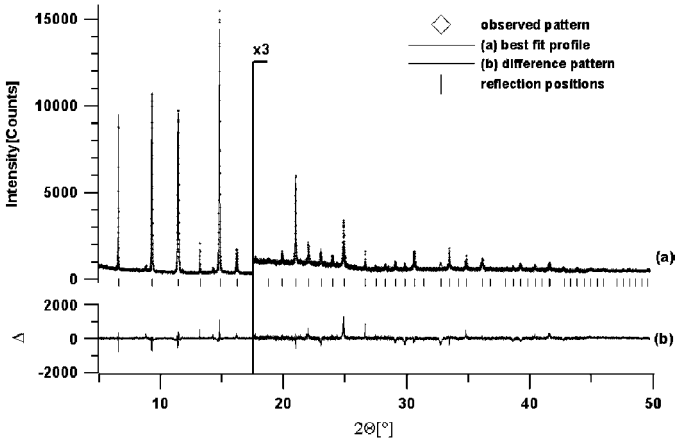

Figure 1
Scattered X-ray intensity for $[Cr(C_7H_8)_2]C_{60}$ at ambient conditions as a function of diffraction angle 2θ. Shown is the observed pattern (diamonds), the best Rietveld-fit profile (line) and the difference curve between observed and calculated profiles. The high-angle part is enlarged by a factor of 3, starting at $2\theta = 17.5°$. The wavelength was $\lambda = 1.15$ Å. The difference between observed and calculated powder patterns can be attributed to deviations from spherical shell electron density for the rotationally disordered molecules.

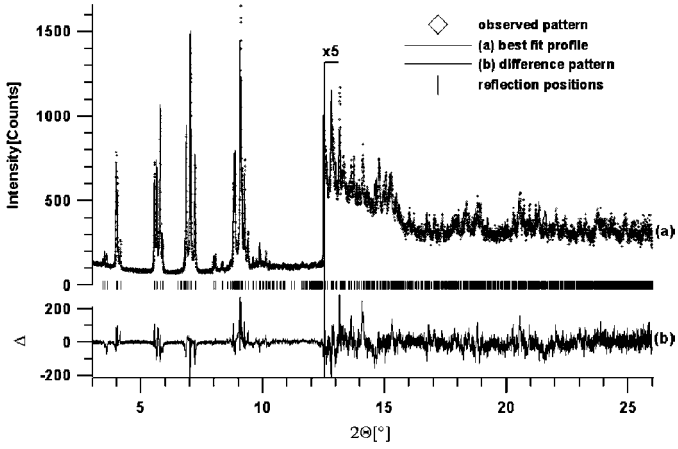

Figure 2
Scattered X-ray intensity for $[Cr(C_7H_8)_2]C_{60}$ at 235 K as a function of diffraction angle 2θ. Shown is the observed pattern (diamonds), the best Rietveld-fit profile (line) and the difference curve between observed and calculated profiles. The high-angle part is enlarged by a factor of 5, starting at $2\theta = 12.5°$. The wavelength was $\lambda = 0.7$ Å.

2. Experimental

X-ray powder diffraction data of the disordered high-temperature phase of $[Cr(C_7H_8)_2]C_{60}$ (Fig. 1) were collected at $T = 295$ K on beamline X3B1 of the Brookhaven National Synchrotron Light Source in transmission geometry with the sample sealed in a 0.7 mm lithium borate glass capillary. X-rays of wavelength 1.15 Å were selected by a double Si(111) monochromator. Wavelengths and the zero point have been determined from eight well defined reflections of the NBS1976 flat plate alumina standard. The diffracted beam was analyzed with a Ge(111) crystal and detected with a Na(Tl)I scintillation counter with a pulse height discriminator in the counting chain. The incoming beam was monitored by an ion-chamber to account for the decay of the primary beam. In this parallel beam configuration, the resolution is determined by the analyzer crystal instead of by slits (Cox, 1992). Data were taken in steps of $\Delta 2\theta = 0.005°$ for 3.2 s from $5 \leq 2\theta \leq 30.0°$ and for 5.2 s from $30 \leq 2\theta \leq 49.76°$. Although θ scans did not show serious crystallite size effects, the sample was spun during measurement for better particle statistics. Several peaks of a very small amount of an unidentified additional phase (< 0.5%) were observed in several peaks in the powder pattern of $[Cr(C_7H_8)_2]C_{60}$.

X-ray powder diffraction data of the ordered low-temperature phase of $[Cr(C_7H_8)_2]C_{60}$ (Fig. 2) were collected for a second sample without noticeable impurities at $T = 235$ K on beamline BM16 at the European Synchrotron Radiation Facility (ESRF) using a Oxford Cryosystems Cryostream cold-nitrogen gas blower. The X-rays from the bending magnet source were collimated vertically by a rhodium-coated silicon mirror before they were incident on the double crystal monochromator. A Si (111) reflection was used to select an X-ray energy of 24 keV. The size of the beam was adjusted to 2×0.6 mm^2 using slits. The wavelength was determined to be 0.7 Å from a silicon standard. The sample was contained in a 0.7 mm lithium borate glass capillary. The sample was spun during measurements in order to improve randomization of the crystallites. The diffracted beam was analyzed with a nine crystal analyzer stage [nine Ge(111) crystals separated by 2° intervals] and detected with nine Na(Tl)I scintillation counters simultaneously. The incoming beam was monitored by an ion-chamber to account for the decay of the primary beam. Data were taken in continuous scanning mode for several hours and they were normalized against monitor counts and detector efficiency and converted to step scan data in steps of $\Delta 2\theta = 0.003°$. Further experimental details are given in Table 1.[1]

Data reduction on both data sets was performed using the *GUFI* (Dinnebier & Finger, 1998) program. Indexing with *ITO* (Visser, 1969) led to a primitive cubic unit cell for the

[1] Supplementary data for this paper are available from the IUCr electronic archives (Reference: SN0020). Services for accessing these data are described at the back of the journal.

Table 1
Crystallographic data for the high- and the low-temperature phase of $[Cr(C_7H_8)_2]C_{60}$.

HT and LT: high- and low-temperature phase; R_p, R_{wp}, R_F, and R_{F^2} refer to the Rietveld criteria of fit for profile and weighted profile respectively, defined in Langford & Louer, 1996).

	HT	LT
Formula	$[Cr(C_7H_8)_2]C_{60}$	$[Cr(C_7H_8)_2]C_{60}$
Temperature (K)	295	235
Formula weight (g mol^{-1})	956.94	1913.88
Space group	$Pm\bar{3}m$	$P\bar{1}$
Z	1	2
a (Å)	9.9840 (1)	13.6414 (8)
b (Å)	9.9840 (1)	13.8338 (7)
c (Å)	9.9840 (1)	13.8548 (7)
α (°)	90	91.830 (3)
β (°)	90	116.776 (2)
γ (°)	90	119.333 (2)
V (Å^3)	995.20 (3)	1924.8 (2)
ρ_{calc} (g cm^{-3})	1.607	1.679
2θ range (°)	5–49.76	3–26.0
Step size (° 2θ)	0.005	0.003
Wavelength (Å)	1.15002 (2)	0.70000 (2)
μ (cm^{-1})	12.01	2.88
R_p	0.061	0.077
R_{wp}	0.086	0.105
R_F	0.267	0.176
R_{F^2}	0.273	0.265
No. of constraints/restraints	6	7
No. of reflections	65	1064

high-temperature phase and a primitive triclinic unit cell for the low-temperature phase with a volume twice as large as that of the cubic phase (lattice parameters in Table 1). The Bragg reflections responsible for the doubling of the triclinic unit cell [(001), (010) and (110)] were very weak. Omitting these peaks led to a triclinic unit cell with dimensions similar to those of the cubic high-temperature phase (a' = 9.9, b' = 9.6, c' = 10.0 Å, α' = 92.5, β' = 92.3, γ' = 89.9°). The number of formula units per unit cell could be determined from packing considerations. It is Z = 1 for the high-temperature phase and Z = 2 for the low-temperature phase. No extinctions were found in both powder patterns, indicating $Pm\bar{3}m$ and $P\bar{1}$ as the most probable space groups, which could later be confirmed by Rietveld refinements (Rietveld, 1969). The peak profiles and precise lattice parameters were determined by Le Bail-type fits (Le Bail *et al.*, 1988) using the programs *GSAS* (Larson & Von Dreele, 1994) and *FULLPROF* (Rodríguez-Carvajal, 1990). The background was modeled manually using *GUFI*. The peak profile was described by a pseudo-Voigt function in combination with a special function that accounts for the asymmetry due to axial divergence (Thompson *et al.*, 1987; Finger *et al.*, 1994). The powder pattern of the cubic high-temperature phase of $[Cr(C_7H_8)_2]C_{60}$ exhibits severe anisotropic peak broadening caused by lattice strain. The sharpest peaks along the [100] direction have a full width at half maximum (FWHM) of 0.0084° 2θ, which is close to the resolution of the diffractometer. The phenomenological strain model of Stephens (1999) as implemented in *GSAS* was used to model the anisotropy of the FWHM. Two parameters were refined for the cubic phase. The resulting anisotropic microstrain distribution is visualized in Fig. 3. Low-angle diffraction peaks of the triclinic low-temperature phase exhibit a FWHM of 0.02° 2θ, an order of magnitude broader than the resolution of the diffractometer.

Approximate positions of the C_{60} and $[Cr(C_7H_8)_2]$ molecules could be directly derived from the metric of the unit cells and packing considerations. Therefore, the next step consisted of Rietveld refinements of the crystal structures of the two phases of $[Cr(C_7H_8)_2]C_{60}$ using the *GSAS* Rietveld refinement package. Since the shape of the C_{60} molecule is known to within very narrow limits, this prior information was used to stabilize the refinements by setting up rigid bodies (Dinnebier, 1999). It is unnecessary to determine this molecular moiety which has a well established structure. In the cubic high-temperature phase, the position of the C_{60} molecule was fixed by symmetry, implying that only three crystallographically distinct atoms were necessary to create the entire C_{60}. In the triclinic low-temperature phase, all 60 C atoms had to be generated. The ratio of the bond lengths C—C/C═C was constrained to 1.0432 with 1.4526 (single bond) and 1.3925 Å (double bond) as initial values (Dinnebier, 1999), leading to a radius of 3.5459 Å. The radius was defined as a refinable parameter. In the cubic high-temperature phase the spherical shell electron density of the C_{60} molecule caused by rotational disorder was sufficiently modeled by simply applying the space-group symmetry to the three C atoms of the rigid body, thus creating a twofold disordered molecule, allowing the rotational parameters of the rigid body to be fixed. This important step reduced the number of refinable parameters for the C_{60} molecule to one (radius) for the cubic phase and seven (three rotations, three translations and the radius) for the triclinic low-temperature phase. Overall temperature

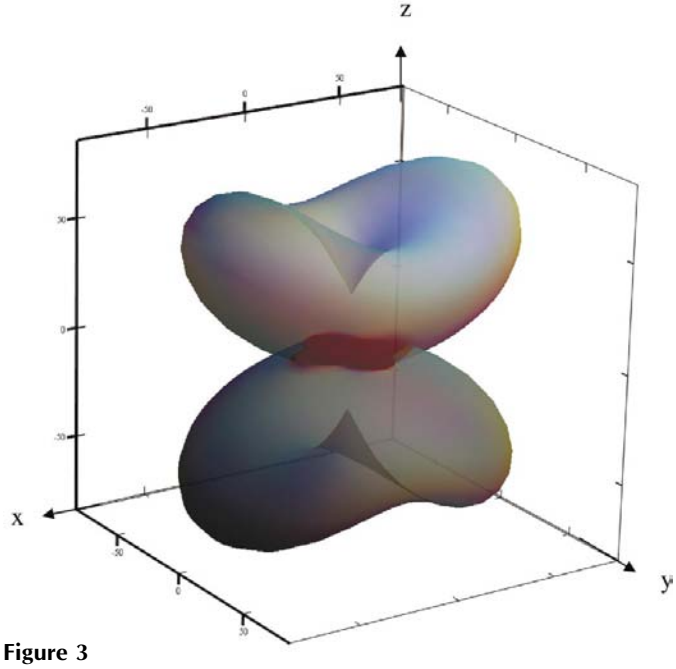

Figure 3
Three-dimenisonal representation of the isosurface of the fourth-order microstrain tensor of $[Cr(C_7H_8)_2]C_{60}$ at ambient conditions.

Table 2
Selected bond lengths (Å) for the high- and low-temperature phase of $[Cr(C_7H_8)_2]C_{60}$.

Distances (Å)	High temperature	Low temperature
C_{60} (C—C)	1.455 (fixed)	1.45 (5)
C_{60} (C═C)	1.394 (fixed)	1.39 (5)
C_{60} (radius)	3.55 (fixed)	3.55 (1) average
C_{59}-C—C-C_{59} (dimer bond)	–	1.55 (5)
C_{60}—C_{60} (centers of gravity)	9.9840 (1)	9.22 (5)
		9.94 (5)
		9.97 (5)
		10.05 (5)
		10.20 (5)

factors were used for the entire C_{60} molecule. The $[Cr(C_7H_8)_2]$ molecule has also been set up as a rigid body with several bond lengths as internal degrees of freedom [C—C, C—H, Cr—$\pi(C_6)$, C—CH_3]. The position of the centrosymmetric $[Cr(C_7H_8)_2]$ molecule was fixed for both phases on inversion centers situated in the middle of the cubic cavities of the primitive cubic packing of the C_{60} molecules, thus prohibiting independent rotation of the two halves of the sandwich complex, which is in accordance with previous reports (Broderick *et al.*, 1997; Braga *et al.*, 1999). In the case of the low-temperature phase, two independent $[Cr(C_7H_8)_2]$ molecules were present. The number of refinable parameters for an individual $[Cr(C_7H_8)_2]$ molecule was reduced to three rotations and four bond lengths, the latter constrained to be equal in both phases. For the disordered high-temperature phase, the bond lengths were fixed at literature values (Starovskii & Struchkov, 1961). During the unconstrained Rietveld refinement of the crystal structure of the low-temperature phase of $[Cr(C_7H_8)_2]C_{60}$, the two C_{60} molecules (related by inversion symmetry) moved towards each other in pairs, thus forming $(C_{60})_2^{2-}$ dimers with a distance of the bonding C atoms of 2.12 Å. Assuming tetrahedral coordination (sp^3 hybridization with a C—C distance of 1.54 Å), the bonding C atoms must be pulled out of the spherical molecular surface by approximately 0.3 Å. To account for the anticipated distortion of the C_{60} molecule, the deviation from the C_{60} radius for the three C atoms, which are adjacent to the bridging C atom, was introduced as an additional degree of freedom of the rigid body. Unconstrained refinement of this parameter resulted in strong correlations to the bond length between the $(C_{60})_2^{2-}$ dimers. The parameter was therefore fixed at literature values (Oszlányi *et al.*, 1996). Lowering the space-group symmetry of the low-temperature phase to *P*1 and refining additional degrees of freedom did not result in an improvement of the refinement. The final difference electron density map was featureless. It should be noted that the quality of the powder pattern of the low-temperature phase of $[Cr(C_7H_8)_2]C_{60}$ is quite low with a peak-to-background ratio of approximately 10:1. The FWHM of the sharpest peak is more than twice the value for the high-temperature phase. Many Bragg reflections are closely overlapping, which explains the relatively high *R* factors of the Rietveld refinements. Positional and isotropic displacement parameters have been deposited.

3. Results and discussion

3.1. Structure description of $[Cr(C_7H_8)_2]C_{60}$

The high-temperature phase of $[Cr(C_7H_8)_2]C_{60}$ crystallizes in a simple CsCl-type structure in which C_{60} represents the chlorine anion and $[Cr(C_7H_8)_2]$ occupies the Cs site. Both constituents are rotationally disordered and can therefore be represented by spheres. The assumption that the fullerene and the chromium complex are rotationally disordered in the high-temperature phase is deduced from NMR results (Hönnerscheid *et al.*, 2001). The radii of the constituents are ~3.3 Å for the bis(toluene)chromium cation (Broderick *et al.*, 1997) and 3.55 Å for the C_{60} molecule (Chow *et al.*, 1992). Thus, the ratio r(cation)/r(anion) = 0.93 is almost the same as for CsCl (Shannon, 1976). This explains geometrically why $[Cr(C_7H_8)_2]C_{60}$ crystallizes in the CsCl-type structure and not in the NaCl-type structure, as usually observed in alkali metal fullerides of the type AC_{60} (A = K, Rb, Cs) at elevated temperatures (Zhu *et al.*, 1993).

Upon cooling below 250 K, cubic $[Cr(C_7H_8)_2]C_{60}$ transforms to a triclinic phase, which consists of ordered $[Cr(C_7H_8)_2]^+$ cations and $(C_{60})_2^{2-}$ anions. The phase transition is reversible and of first order. Thermal analysis of the phase transition confirms the claimed reversibility, as can be seen by the identical shape of the four temperature cycles plotted superimposed in Fig. 4. From the small hysteresis of the phase transition and the temperature dependency of the molar volume (not shown), the phase transition is deduced to be of first order.

The crystal structure of the dimer phase of $[Cr(C_7H_8)_2]C_{60}$ is compared with the crystal structure of the dimer phase of RbC_{60} in Fig. 5. The dimer direction coincides with the shortest C_{60}—C_{60} distance, *i.e.* the [001] direction of the former cubic lattice and the [011] direction of the triclinic lattice, respectively. It is noteworthy that the direction of the dimer bond in the triclinic phase is equivalent to the direction

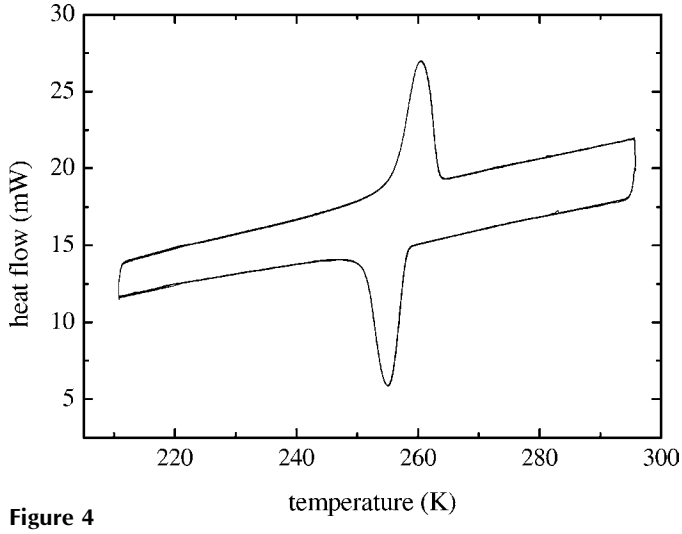

Figure 4
Thermal analysis of the phase transition of $[Cr(C_7H_8)_2]C_{60}$. Four cycles are plotted superimposed and all show identical shape. The heating/cooling rate is 10 K min^{-1}.

of the smallest microstrain in the cubic high-temperature phase, as depicted in Fig. 3. Microstrain is directly related to the elastic constants of the material. As a fourth-rank covariant tensor, the elasticity is anisotropic even for cubic crystal symmetry. In the case of the cubic phase of $[Cr(C_7H_8)_2]C_{60}$ one can say that the compressibility along the direction in which the dimerization occurs is almost one magnitude lower than along the face diagonals. The basic primitive cubic (p.c.) arrangement of C_{60} molecules is preserved in the low-temperature phase. The structure can thus be described as consisting of slightly distorted cubes of C_{60} with bis(toluene)chromium in each cubic cavity. Two opposite edges of each cube are markedly shortened, leading to single-bonded C_{60} dimers. The distances between the centers of gravity of the C_{60} molecules are 9.22 (5) Å for the dimer and 9.94 (5)–10.20 (5) Å for the other directions. For comparison, the distance in the cubic phase is 9.9840 (1) Å, which is considered the typical van der Waals distance between C_{60} monomers (Heiney *et al.*, 1991). Selected distances of both phases are listed in Table 2. The transformation matrix from the cubic lattice of the high-temperature phase to the triclinic lattice of the low-temperature phase is given by

$$\begin{pmatrix} -1 & 0 & 1 \\ 1 & -1 & 0 \\ 1 & 1 & 0 \end{pmatrix},$$

accompanied by a shift of origin of

$$\begin{pmatrix} 1/2 \\ 0 \\ 0 \end{pmatrix}.$$

As can be seen from Fig. 5 the $[Cr(C_7H_8)_2]^+$ cations show two different orientations in the structure of the low-temperature phase, which can be attributed to steric reasons. As mentioned above, a distorted cube of C_{60} molecules exhibits two short edges representing the intermolecular C_{60} bonds. Both chromium complexes with their bulky toluene ligands orient along a body diagonal of the cube connecting the long edges of the cube. Adjacent cubes are not identical in the dimer phase: they can be transformed into one another by rotation of 90° about a direction parallel to the dimer bond, implying that the chromium complexes orient differently in neighboring cubes.

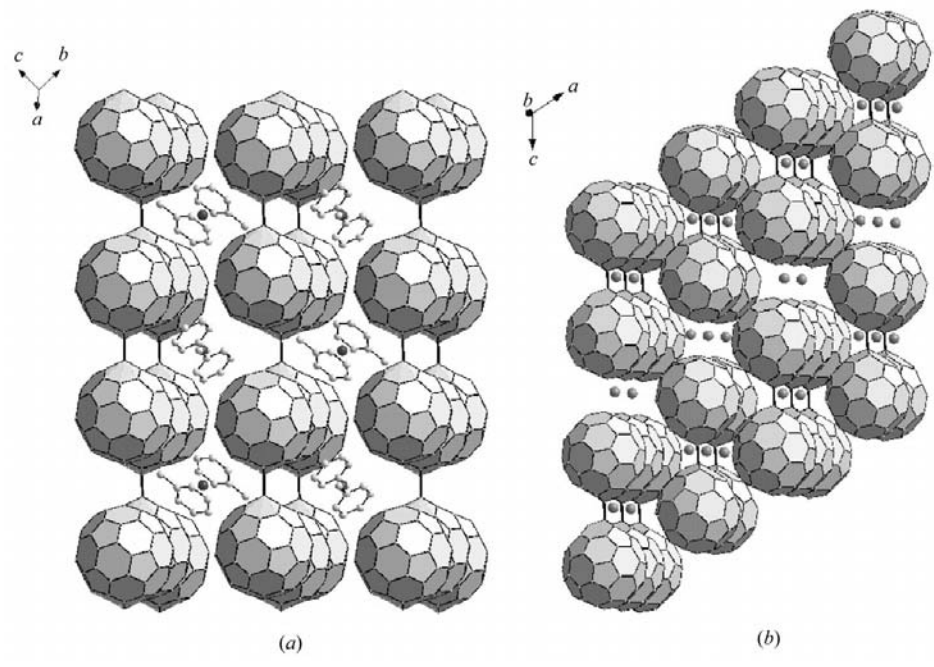

Figure 5
(*a*) Crystal structure of the low-temperature phase of $[Cr(C_7H_8)_2]C_{60}$ in a view towards (610). For lucidity only half of the bis(toluene)chromium molecules are shown. (*b*) Crystal structure of monoclinic RbC_{60} (Oszlányi *et al.*, 1996) viewed along the *b* axis. The dimer bonds are drawn in bold.

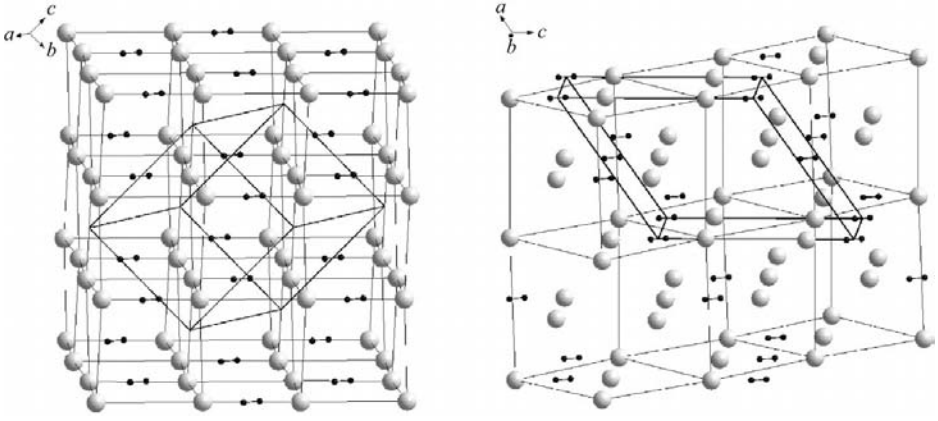

Figure 6
Comparison of the dimer phases of $[Cr(C_7H_8)_2]C_{60}$ (left) and RbC_{60} (right). The large gray spheres represent the centers of gravity of the C_{60} molecules. The black dumbbells show the arrangement of the dimer bonds. The unit cells of the low-temperature phases (bold lines) as well as of the corresponding high-temperature phases (thin lines) are drawn.

3.2. Comparison with alkali metal fullerides

The dimer formation of fullerides was first discovered in alkali metal fullerides of the type AC_{60} (A = K, Rb, Cs), see Zhu *et al.* (1995). In contrast to the alternative [2 + 2] cycloaddition of C_{60} molecules, the dimers are linked by a single carbon–carbon bond. In the following we want to emphasize the similarities and differences between RbC_{60} (Oszlányi *et al.*, 1996) and $[Cr(C_7H_8)_2]C_{60}$. In the high-temperature rocksalt-type structure of RbC_{60} (space group $Fm\bar{3}m$) the Rb atoms occupy the

octahedral cavities in the f.c.c. packing of C_{60} molecules. In the high-temperature phase of bis(toluene)chromium fulleride the rotationally disordered $[Cr(C_7H_8)_2]$ molecules occupy the cubic voids in the p.c. arrangement of the C_{60} molecules. Upon cooling below $T = 250$ K for $[Cr(C_7H_8)_2]C_{60}$ and $T = 270$ K for RbC_{60}, both compounds undergo a first-order phase transition forming dimers of C_{60} molecules. In the case of RbC_{60}, quenching is necessary to reach the metastable dimer phase (space group $P2_1/a$) by an irreversible phase transition, whereas in the case of $[Cr(C_7H_8)_2]C_{60}$ a reversible phase transition towards a thermodynamically stable dimer phase (space group $P\bar{1}$) occurs, independently of the cooling speed. In the low-temperature phases of both $[Cr(C_7H_8)_2]C_{60}$ and RbC_{60} the basic packing principle of the high-temperature phases is retained. The lengths of the dimer bonds ($\simeq 1.5$ Å) are equal for both compounds within the accuracy of the measurements. Furthermore, in both cases, the centers of the dimer bonds lie on centers of symmetry, thus relating the two interconnected C_{60} molecules by inversion symmetry. Fig. 6 shows the dimer arrangement in $[Cr(C_7H_8)_2]C_{60}$ and RbC_{60}, including the cell dimensions of the dimer phases and of the former cubic phases. The dimer formation occurs in both phases along the shortest $C_{60}-C_{60}$ distances of the cubic high-temperature phases, namely the [001] direction for $[Cr(C_7H_8)_2]C_{60}$ and [110] for RbC_{60}. The arrangement of the C_{60} molecules in both crystal structures can be described as rods of C_{60} molecules with short and long distances alternating. Whereas in $[Cr(C_7H_8)_2]C_{60}$ each rod is surrounded by four neighboring rods (tetragonal rod packing), in RbC_{60} each rod has six nearest-neighbor rods (hexagonal rod packing), corresponding to the different packing schemes of the C_{60} molecules in the high-temperature phases. In $[Cr(C_7H_8)_2]C_{60}$ a short distance (single bond) in a rod faces long distances in the four neighboring rods and *vice versa*. A dimer bond in RbC_{60} faces two dimer bonds in the crystallographic *b* direction of the monoclinic unit cell and four C_{60} molecules perpendicular to the dimer direction.

4. Conclusions

Using high-resolution X-ray powder diffraction, it was possible to fully characterize the crystal structures of the low- and high-temperature phase of $[Cr(C_7H_8)_2]C_{60}$. In particular, the consequent use of rigid bodies in Rietveld analysis allowed the determination of the crystal structure of the low-temperature phase of $[Cr(C_7H_8)_2]C_{60}$ from a low-quality powder pattern, suffering from low crystallinity of the sample at low temperatures. In contrary to the common f.c.c. arrangement of C_{60} anions in alkali fullerides, the structures of $[Cr(C_7H_8)_2]C_{60}$ are based on a p.c. arrangement of C_{60} molecules. For the first time the formation of C_{60} dimers was found to occur through a reversible first-order phase transition. Besides information on the microstrain distribution within cubic $[Cr(C_7H_8)_2]C_{60}$, the analysis of anisotropic peak broadening from a Le Bail type of fit, simply using the metric information of the crystal lattice, allowed the prediction of the possible direction for dimerization.

Research was carried out in part at the National Synchrotron Light Source at Brookhaven National Laboratory, which is supported by the US Department of Energy, Division of Materials Sciences and Division of Chemical Sciences. The SUNY X3 beamline at NSLS is supported by the Division of Basic Energy Sciences of the US Department of Energy under Grant No. DE-FG02-86ER45231. Special thanks to Peter Stephens (SUNY at Stony Brook) and Andy Fitch (ESRF) for their assistance during data collection. Research at ESRF was carried out under general user proposal CH-1036. Financial support by the Deutsche Forschungsgemeinschaft (DFG) and the Fonds der Chemischen Industrie (FCI) is gratefully acknowledged.

References

Braga, D., Draper, S. M., Champeil, E. & Crepioni, F. (1999). *J. Organomet. Chem.* **573**, 73–77.
Broderick, W. E., Choi, K. W. & Wan, W. C. (1997). *Electrochem. Soc. Proc.* **14**, 1102–1115.
Chauvet, O., Oszlányi, G., Forró, L., Stephens, P. W., Tegze, M., Faigel, G. & Jánossy, A. (1994). *Phys. Rev. Lett.* **72**, 2721–2724.
Chow, P. C., Jiang, X., Reiter, G., Wochner, P., Moss, S. C., Axe, J. D., Hanson, J. C., McMullan, R. K., Meng, R. L. & Chu, C. W. (1992). *Phys. Rev. Lett.* **69**, 2943–2946.
Cox, D. E. (1992). *Synchrotron Radiation Crystallography*, edited by P. Coppens, ch. 9, pp. 186–254. New York: Academic Press.
Dinnebier, R. E. & Finger, L. (1998). *Jahrestagung der Deutschen Gesellschaft für Kristallographie (DGK)*. Collected abstracts, 148, Karlsruhe, 2–5 March 1998.
Dinnebier, R. E. (1999). *Powder Diffr.* **14**, 84–92.
Finger, L. W., Cox, D. E. & Jephcoat, A. P. (1994). *J. Appl. Cryst.* **27**, 892–900.
Fox, J. R., Lopinski, G. P., Lannin, J. S., Adams, G. B., Page, J. B. & Fischer, J. E. (1996). *Chem. Phys. Lett.* **249**, 195–200.
Heiney, P. A., Fischer, J. E., McGhie, A. R., Romanow, W. J., Denenstein, A. M., McCauley Jr, J. P. & Smith III, A. B. (1991). *Phys. Rev. Lett.* **66**, 2911–2914.
Hönnerscheid, A., van Wüllen, L., Jansen, M., Rahmer, J. & Mehring, M. (2001). *J. Chem. Phys.* **115**, 7161–7165.
Iwasa, Y., Arima, T., Fleming, R. M., Siegrist, T., Zhou, O., Haddon, R. C., Rothberg, L. J., Lyons, K. B., Carter Jr, H. L., Hebard, A. F., Tycko, R., Dabbagh, G., Krajewski, J. J., Thomas, G. A. & Yagi, T. (1994). *Science*, **264**, 1570–1572.
Langford, I. & Louër, D. (1996). *Rep. Prog. Phys.* **59**, 131–234.
Larson, A. C. & Von Dreele, R. B. (1994). *GSAS*. Los Alamos National Laboratory Report LAUR 86-748. (Used version: August 1997).
Le Bail, A., Duroy, H. & Fourquet, J. L. (1988). *Mater. Res. Bull.* **23**, 447–452.
Núñez-Regueiro, M., Marques, L., Hodeau, J.-L., Béthoux, O. & Perroux, M. (1995). *Phys. Rev. Lett.* **74**, 278–280.
Oszlányi, G. & Forró, L. (1995). *Solid State Commun.* **93**, 265–267.
Oszlányi, G., Bortel, G., Faigel, G., Gránásy, L., Bendele, G. M., Stephens, P. W. & Forró, L. (1996). *Phys. Rev. B*, **54**, 11849–11852.
Oszlányi, G., Baumgartner, G., Faigel, G. & Forró, L. (1997). *Phys. Rev. Lett.* **78**, 4438–4441.

Prassides, K., Vavekis, K., Kordatos, K., Tanigaki, K., Bendele, G. M. & Stephens, P. W. (1997). *J. Am. Chem. Soc.* **119**, 834–835.
Rao, A. M., Zhou, P., Wang, K., Hager, G. T., Holden, J. M., Wang, Y., Lee, W.-T., Bi, X., Eklund, P. C., Cornett, D. S., Duncan, M. A. & Amster, I. J. (1993). *Science*, **259**, 955–957.
Rietveld, H. M (1969). *J. Appl. Cryst.* **2**, 65–71.
Rodríguez-Carvajal, J. (1990). Abstracts of the Satellite Meeting on Powder Diffraction of the XV Congress of the IUCr, p. 127. Toulouse, France.
Shannon, R. D. (1976). *Acta Cryst.* A**32**, 751–767.
Starovskii, O. V. & Struchkov, Y. T. (1961). *Zh. Strukt. Khim.* **2**, 162.
Stephens, P. W., Bortel, G., Faigel, G., Tegze, M., Jánossy, A., Pekker, S., Oszlányi, G. & Forro, L. (1994). *Nature*, **370**, 636–639.
Stephens, P. W. (1999). *J. Appl. Cryst.* **32**, 281–289.
Thompson, P., Cox, D. E. & Hastings, J. B. (1987). *J. Appl. Cryst.* **20**, 79–83.
Visser, J. W. (1969). *J. Appl. Cryst.* **2**, 89–95.
Zhu, Q., Zhou, O., Fischer, J. E., McGhie, A. R., Romanow, W. J., Strongin, R. M., Cichy, M. A. & Smith III, A. B. (1993). *Phys. Rev. B*, **47**, 13948–13951.
Zhu, Q., Cox, D. E. & Fischer, J. E. (1995). *Phys. Rev. B*, **51**, 3966–3969.